American Journal of Pathology, Vol. 151, No. 6, December 1997

Analysis of Apoptosis during Hair Follicle Regression (Catagen)

Gerd Lindner, Vladimir A. Botchkarev, Natalia V. Botchkareva, Gao Ling, Carina van der Veen, and Ralf Paus

From the Department of Dermatology, Charité, Humboldt-Universität zu Berlin, Berlin, Germany

Keratinocyte apoptosis is a central element in the regulation of hair follicle regression (catagen), yet the exact location and the control of follicular keratinocyte apoptosis remain obscure. To generate an "apoptomap" of the hair follicle, we have studied selected apoptosis-associated parameters in the C57BL/6 mouse model for hair research during normal and pharmacologically manipulated, pathological catagen development. As assessed by terminal deoxynucleotide transferase dUTP fluorescein nick end-labeling (TUNEL) stain, apoptotic cells not only appeared in the regressing proximal follicle epithelium but, surprisingly, were also seen in the central inner root sheath, in the bulge/isthmus region, and in the secondary germ, but never in the dermal papilla. These apoptosis hot spots during catagen development correlated largely with a down-regulation of the Bcl-2/Bax ratio but only poorly with the expression patterns of interleukin-1β converting enzyme, $p55^{TNFR}$, and Fas/Apo-1 immunoreactivity. Instead, a higher correlation was found with $p75^{NTR}$ expression. During cyclophosphamide-induced follicle dystrophy and alopecia, massive keratinocyte apoptosis occurred in the entire proximal hair bulb, except in the dermal papilla, despite a strong up-regulation of Bax and $p75^{NTR}$ immunoreactivity. Selected receptors of the tumor necrosis factor/nerve growth factor family and members of the Bcl-2 family may also play a key role in the control of follicular keratinocyte apoptosis *in situ*. *(Am J Pathol 1997, 151:1601–1617)*

One of the most intriguing features of the hair follicle is that, after a prolonged period of growth (anagen), it spontaneously enters into a phase of rapid organ involution (catagen) until the follicle re-enters into anagen via an interspersed resting phase (telogen).[1,2] Based on morphological evidence, this organ involution, to a large extent, reflects coordinated keratinocyte apoptosis in the regressing proximal hair bulb.[3] No other mammalian organ rhythmically undergoes such dramatic, but physiological, apoptosis during the entire lifespan of the organism. Thus, catagen development offers one of the most attractive models available to date for studying the controls of programmed epithelial cell death *in situ* in fully developed mammalian organisms.[4,5] As is the case in numerous other developmental systems,[6] apoptosis is also an important parameter for modeling the architecture of the developing follicle epithelium during follicle morphogenesis.[5,7]

However, the occurrence of cell death in normal catagen with the light microscopic and ultrastructural features of apoptosis[3] has not yet been confirmed by standard biochemical evidence, using, eg, the *in situ* end-labeling technique (terminal deoxynucleotide transferase (TdT) dUTP fluorescein nick end labeling (TUNEL)) or by demonstrating endonuclease activation.[8,9] Neither have the subpopulations and the exact intrafollicular location of apoptotic follicle cells during the various stages of normal catagen been defined, nor have the controls of follicle keratinocyte apoptosis during spontaneous catagen been elucidated. In fact, most of our current understanding of the regulation of apoptosis is based on *in vitro* studies of hematopoietic, neural, and transformed cell populations,[10–13] whereas very little is known on the control of normal keratinocyte apoptosis *in situ*.[4,7,14]

In mice, the steady-state mRNA levels for some gene products implicated in the control of apoptosis, eg, Fas, transforming growth factor (TGF)-β, and tumor necrosis factor (TNF)-β, rise when a wave of follicles enters into the anagen-catagen-telogen transformation of the hair cycle.[15] In sheep, the infusion of epidermal growth factor (EGF) induces synchronized catagen by triggering massive keratinocyte apoptosis in the proximal hair bulb,[16,17] and multiple additional signaling molecules have been implicated in the control of catagen, eg, fibroblast growth factor (FGF)-5, TGF-β, insulin-like growth factor (IGF)-1, parathyroid hormone-related peptide (PTHrp) (for review see Refs. 18 and 19). Yet it has not been clarified for any of these factors which direct role they play in the control of follicle keratinocyte apoptosis *in situ*.

Therefore, one basic challenge remains to define the location of apoptotic cells during follicle regression and to correlate this with key parameters likely to be relevant

Supported by the Deutsche Krebshilfe (W1/94/Pa 1), and the Deutsche Forschungsgemeinschaft (Pa 345/3–2).

Accepted for publication August 26, 1997.

Address reprint requests to Dr. Ralf Paus, Department of Dermatology, Charité, Humboldt-Universität, D-10117, Berlin, Germany. E-mail: ralfpaus@ukrv.de.

in the control of keratinocyte apoptosis. Apoptosis underlies strict "social controls"[20] exerted by the cellular microenvironment and probably reflects the net result of a wide range of interacting extra- and intracellular, pro- and anti-apoptotic factors.[12,13,21–23] Thus, follicular apoptosis may result from the coincidence of a decline of anti-apoptotic factors (eg, decreased receptor expression for growth factors that suppress apoptosis and declining intracellular Bcl-2 level) with an increase in pro-apoptotic factors (eg, increased expression of "death receptors" such as Fas/Apo-1, $p55^{TNFR}$, and $p75^{NTR}$ and increase of intracellular Bax level and interleukin-1β converting enzyme (ICE) activity) during the final period of the growth phase (late anagen VI).[18,24]

To probe this hypothesis, we have studied catagen-associated apoptosis in the C57BL/6 mouse model for hair research.[1,25,26] We have assessed when and where exactly apoptotic cells can be visualized during the spontaneous catagen transformation of depilation-induced anagen VI follicles,[26–28] whether there are signs of endonuclease activity[9,22] during normal and pathological catagen development, and how this correlates with the expression of Bcl-2, Bax, ICE, Fas, $p55^{TNFR}$, and $p75^{NTR}$. The latter parameters were selected for analysis as the intracellular ratio of anti-apoptotic Bcl-2 and pro-apoptotic Bax expression is considered to be one critical factor in apoptosis control[13,21,22,29] and because activation of members of the ICE-like cysteine protease family is thought to represent a fairly late, irreversible key event in the apoptosis control machinery.[23,30,31] Selected members of the TNF/nerve growth factor (NGF) receptor family[32] were studied, as they are involved in the initiation of apoptosis by their corresponding ligands in multiple cell types: Fas/Apo-1,[11,30,33] $p55^{TNFR}$,[34,35] and $p75^{NTR}$.[36–38]

To compare the expression patterns of these intrafollicular apoptosis-related parameters during physiological catagen with those observed during pathological catagen development, two additional, pharmacologically manipulated types of anagen-catagen transformation were studied: 1) massive, premature, but morphologically normal catagen induced by topical dexamethasone[27] (DEX) and 2) dystrophic, premature catagen development associated with alopecia, induced by systemic cyclophosphamide (CYP).[39–41] These comparisons are interesting in that they allow insights into conditions under which follicle keratinocyte apoptosis occurs in an exaggerated manner[42–43] and in that they offer clinically relevant models for human hair growth disorders (DEX-induced catagen: telogen effluvium;[27] CYP: chemotherapy-induced alopecia[39]). On this basis, novel strategies for the prevention of intrafollicular apoptosis might then be developed, which target defined controls of follicle keratinocyte apoptosis.

Materials and Methods

Animal Model and Tissue Collection

Six- to nine-week-old, syngeneic, female C57BL/6 mice in the telogen stage of the hair cycle, weighing 15 to 20 g, were purchased from Charles River (Sulzfeld, Germany), housed in community cages at the animal facilities of the Virchow Hospital (Berlin, Germany) with 12-hour light periods, and fed water and mouse chow *ad libitum*. The growth phase of the hair cycle (anagen) was induced in the back skin of mice with all follicles in the resting phase of the hair cycle (telogen), as judged from their homogeneously pink back skin color, by application of a melted wax/rosin mixture (1:1) under general anesthesia as previously described.[26,27] Briefly, after hardening, the wax/rosin mixture was peeled off the skin, thus plucking all telogen hair shafts and thereby inducing the follicles to enter anagen.

After 17 to 19 days, these depilation-induced anagen follicles enter spontaneously into catagen, as can be appreciated from the conversion of their skin color from black to gray and finally to pink. This transformation begins in the neck region and travels to the tail region and flanks within 2 to 3 days until the entire depilated back area is pink again (ie, in telogen).[1,27] All stages of the anagen VI/catagen I to VIII/telogen transformation of the murine hair cycle were studied (classification according to Ref. 1), with special emphasis on anagen VI (12 and 16 days after depilation (p.d.)) and catagen II, IV, VI, and VII (17, 18, and 19 days p.d.).[27,28]

Spontaneous catagen development in depilation-induced anagen follicles was compared with massive, premature, but morphologically normal, catagen development that had been induced by topical 0.1% DEX-21-acetate application[27] and with premature, pathological, dystrophic catagen associated with alopecia, as induced by CYP intraperitoneally.[39,40]

The neck region of murine back skin was harvested parallel to the vertebral line to obtain longitudinal sections through the hair follicles[25] and was deep frozen in liquid nitrogen, covered with embedding medium, and processed for immunohistochemistry and TUNEL staining as described below. In general, each parameter was examined by studying at least 50 hair follicles of at least three different mice per cycle stage.

TUNEL/Hoechst 33242

To evaluate apoptotic cells, we used an established, commercially available TUNEL kit (ApopTag, Oncor, Gaithersburg, MD). In addition, we combined this procedure with counterstaining by HOECHST 33342 dye (Sigma Chemical Co., Diesenhofen, Germany), which intercalates between DNA base pairs and can be used for detecting apoptotic cells that become visible as shrunken or fragmented, intensively labeled cells or apoptotic bodies.[9] Using this combined technique, which increases the likelihood of correct identification of apoptotic cells, apoptotic cells were identified by comparing shrunken, intensively stained nuclei and fragmented chromatin with surrounding, normal cells. As a high rate of constitutive apoptosis prominently occurs in thymocytes,[31,45,46] the same procedure was carried out with thymus cryosections of 4-week-old mice as positive controls.

Ten-micron cryostat sections of C57BL/6 back skin were freshly prepared and fixed in formalin (10%) for 10

Table 1. Antibodies: Source, Technique, and Dilution

Antigen	Characterization of primary antibody	Dilution	Reference	Technique	Source
ICE	Polyclonal rabbit-anti-mouse, recognizes an amino acid sequence of inactive ICE and of the p10 subunit of activated ICE	1:100	50, 51	IF	Santa Cruz Biotechnology, Santa Cruz, CA
Bcl-2	Monoclonal hamster anti-mouse Bcl-2 p26 protein	1:250	76	ABC	Pharmingen, San Diego, CA
Bax	Monoclonal rat anti-mouse Bax-α 21-kd protein	1:250	77	APAAP	Pharmingen
Fas/Apo-1	Monoclonal hamster anti-mouse Fas/Apo-1 45-kd cell surface protein	1:50	78	ABC	Pharmingen
$p55^{TNF}$	a) Polyclonal goat anti-human TNF receptor binding protein I	1:100	79	ABC	R&D Systems, Minneapolis, MN
	b) Monoclonal rat anti-mouse TNF receptor ($p55^{TNFR}$)	1:20		APAAP	Biozol, Eching, Germany
$p75^{NTR}$	Monoclonal rat anti-mouse $p75^{NTR}$ receptor	1:100	80	APAAP	Chemicon, Temecula, CA

IF, immunofluorescence; APAAP, alkaline phosphatase anti-alkaline phosphatase; ABC, avidin-biotin complex.

minutes at room temperature (RT) and post-fixed in ethanol/acetic acid (2:1) for 5 minutes at −20°C. The sections were then covered with equilibration buffer for 5 minutes at RT, followed by an incubation with TdT solution for 1 hour at 37°C. The reaction was terminated with stop/wash buffer (30 minutes at 37°C). Digoxigenin-dUTP-labeled DNA compounds were detected by anti-digoxigenin fluorescein isothiocyanate (FITC)-conjugated $F(ab)_2$ fragments. Dilutions used for the TUNEL stain were adopted from the manufacturer's manual. Counterstaining with HOECHST 33342 dye (10 μg/ml in phosphate-buffered saline (PBS)) was performed by an incubation step of 45 minutes at RT. Each phase was interspersed by a washing step (three times) in PBS. Finally, sections were mounted using VectaShield (Vector Laboratories, Burlingame, CA), and apoptotic cells were detected with a fluorescence microscope (Zeiss, Jena, Germany) with the appropriate filters. Negative controls for the TUNEL staining were made by omitting TdT, according to the manufacturer's protocol. Positive TUNEL controls were run by comparison with tissue sections from the thymus of young mice, with their high degree of spontaneous thymocyte apoptosis.

Quantitative Histomorphometry

The number of TUNEL-positive cells per follicle in four different regions (bulge/isthmus, central inner root sheath, proximal hair bulb, and epithelial strand) was counted at four different time points (late anagen VI, catagen II, catagen IV, and catagen VII) of the murine hair cycle. The graph shown in Figure 4 was derived from analyzing >20 longitudinally sectioned follicles from the lower back of three C57BL/6 mice per time point. Note that the epithelial strand does not appear before catagen VI has developed and that the proximal hair bulb is deleted by catagen VII.[1]

DNA Laddering

DNA laddering was examined using standard protocols.[9,22] DNA was extracted (DNA extraction kit, Stratagene, La Jolla, CA) from full back skin harvested at various time points of the C57BL/6 murine hair cycle, with or without pharmacological treatment (CYP or DEX). Apoptosis induction by 1 nmol/L camptothecin[47] in HL-60 cells and DNA extracts from the thymus of 4-week-old mice were used as controls. DNA content was evaluated by photometric detection (UV_{260}), and the same amount of DNA was loaded in each lane. DNA laddering was visualized using a 2% agarose gel containing ethidium bromide (0.5 μg/ml), and documentation was done by using a Polaroid camera. The 400-bp band of each lane was evaluated by computer-assisted scanner densitometry (ScanPack, Biometra, Göttingen, Germany).

Immunohistochemistry

The primary and secondary antibodies used here, their dilutions, and the antibody sources are outlined in Table 1. As no control peptides were available for preabsorption negative control (except in the case of ICE), incubation with the appropriate serum without primary antibodies was used as negative control. In addition, systematic comparison of the observed immunoreactivity (IR) patterns with published IR patterns of the stained antigens were taken as internal positive and negative controls for each antibody.

All specific and reproducible IR patterns were recorded and summarized in computer-generated schematic representations of the anagen-catagen transformation of the murine hair cycle, designed to reflect the key features of murine hair follicle anatomy and their changes during catagen development as accurately as possible. These qualitative summary schemes shown below reflect only the most prominent and most reproducible, specific IR patterns identified by three independent observers. To determine whether individual cell populations showed IR for multiple antigens, double and triple stains were performed according to our previously described immunohistology and immunofluorescence protocols.[48,49] Photomicrographs of all immunohistological analyses were generated using a Zeiss microscope and a digital image analysis system (Isis, Metasystems, Altlussheim, Germany).

Interleukin-1β Converting Enzyme (ICE)

To determine which cell populations co-express ICE IR with signs of DNA fragmentation, the combined Hoechst 33342 and *in situ* end labeling method (TUNEL) described above and an immunohistochemical staining method for ICE IR detection were combined. The ICE antibody recognizes the p10 subunit of activated ICE and an amino acid sequence of inactive ICE.[50,51]

In the first part of this triple-staining protocol, the TUNEL reaction was performed as described above, except for addition of the anti-digoxigenin FITC-conjugated $F(ab)_2$ fragments (omission of the final step). Sections were then blocked with 10% normal goat serum in 0.05 mol/L Tris-buffered saline (TBS) for 20 minutes at RT and were incubated overnight (without an interspersed washing step) with anti-ICE antibody (containing 2% normal goat serum in TBS). After a subsequent washing step, sections were incubated with anti-digoxigenin FITC-conjugated $F(ab)_2$ fragments. The secondary antibody (goat anti-rabbit tetraethylrhodamine-isothiocyanate-conjugated $F(ab)_2$ fragments, 1:200) was incubated for 30 minutes at 37°C after an additional interspersed washing step. As negative control, neutralizing peptide (1:50 in PBS; Santa Cruz Technologies, Santa Cruz, CA) was preincubated with anti-ICE antibody for 1 hour at 37°C. The distribution and intensity of ICE-immunoreactive (ICE-IR) cells were determined with a fluorescence microscope (Zeiss, using the appropriate filters) at magnifications from ×100 to ×400.

Bcl-2/Bax

Bcl-2 and Bax antigens were detected by a double-staining procedure (Table 1). Ten-micron cryostat sections were fixed in acetone (10 minutes at −20°C) and preincubated with 10% normal bovine serum (NBS), followed by an incubation with the primary anti-Bax antibody overnight containing 1% NBS. After washing, sections were incubated with rabbit anti-rat secondary antibody (1:200), containing 2% normal rabbit serum and 4% normal mouse serum. After an additional washing step, sections were incubated with rat alkaline phosphatase anti-alkaline phosphatase complex (Dako, Glostrup, Denmark) in the same buffer as the secondary antibody. To increase staining intensity, the last two steps were repeated for 10 minutes each. For the developing of the first color reaction, Fast Blue (Sigma) was prepared according to the manufacturer's protocol, and sections were incubated for 15 to 20 minutes after an additional washing step. In the second part of the double-staining procedure, avidin and biotin blocking solution (Vector Laboratories) was added for 15 minutes each, interspersed with washing. Sections were then incubated overnight with anti-mouse Bcl-2 antibody (containing 2% NBS). After a subsequent washing step, the secondary antibody (goat anti-hamster, diluted 1:200 and containing 4% normal goat serum) was added to the sections for 30 minutes. Avidin-biotin complex (ABC) solution (Vector Laboratories), labeled with horseradish peroxidase, was prepared (avidin and biotin, each 1:100) 30 minutes before use and was then incubated for 30 minutes after washing. The 3-amino-9-ethylcarbazole (Sigma) developing solution was prepared as previously described,[48] and the color reaction was performed for 15 to 20 minutes after an additional washing step. Finally, Kaiser's aqueous gelatin glycerol was used for mounting the slides. In addition, selected sections were also stained using only antibody against Bcl-2 according to the protocol described above, and in this case, ABC/alkaline phosphatase was used at the last step of immunohistochemical procedure, and cell nuclei were counterstained by Meyer's hemalaun. Reactions were performed at RT, and TBS was used for washing and to dilute the antibodies. The distribution of Bax IR was assessed by blue, and Bcl-2 IR was assessed by red or red/brown color, using a light microscope (Zeiss).

Fas/APO-1, $p55^{TNFR}$, and $p75^{NTR}$

The IR patterns of each of these apoptosis-associated cell surface receptors were evaluated by immunohistology. To judge the results of the antibody against human TNF receptor-binding protein I (Table 1, $p55^{TNFR}$ (a)), we used an additional antibody directed to mouse $p55^{TNFR}$ antigen (Table 1, $p55^{TNFR}$ (b)). Fas/APO-1 and $p55^{TNFR}$ (a) IR was assessed by the same techniques. The same protocol as described in the first part of the Bcl-2/Bax double staining was used for the second primary antibody (b) against the $p55^{TNFR}$ antigen listed in Table 1.

Ten-micron cryostat sections of each selected hair cycle stage were prepared as described above and then blocked with avidin and biotin (Vector Laboratories) for 15 minutes each. In addition, sections were blocked either with 10% NBS in TBS for 15 minutes (for Fas/Apo-1) or with 10% normal swine serum, 1% normal mouse serum, and 1% NBS (for $p55^{TNFR}$). Without washing, sections were then incubated with primary antibody ($p55^{TNFR}$ and Fas/Apo-1) overnight, followed by an incubation (30 minutes at 37°C) with biotinylated secondary antibody (1:200), containing 1% NBS (for $p55^{TNFR}$) or 4% normal goat serum (Fas/Apo-1). Alkaline-phosphatase-conjugated streptavidin was used as a third-layer reagent (diluted 1:500 in TBS for 7 minutes at 37°C). $p75^{NTR}$ antigen was detected using the same protocol as described in the first part of the Bcl-2/Bax double staining, using the primary antibody listed in Table 1. Antigen/antibody complexes were visualized using the previously described developing solution.[52] The color reaction was stopped 10 to 15 minutes later in TBS after standard counterstaining (Meyer's). Incubations were done at RT, followed by washing with TBS for 5 minutes (three times). Slides were mounted in Kaiser's aqueous gelatin glycerol. Positive staining was identified by a red color.

Results

Distribution of TUNEL-Positive Cells during the Anagen-Catagen Transformation

Double staining by the TUNEL method and Hoechst 33342 dye revealed that almost all TUNEL-positive cells in the follicle epithelium also showed a substantial increase in the intensity of Hoechst 33342 staining (com-

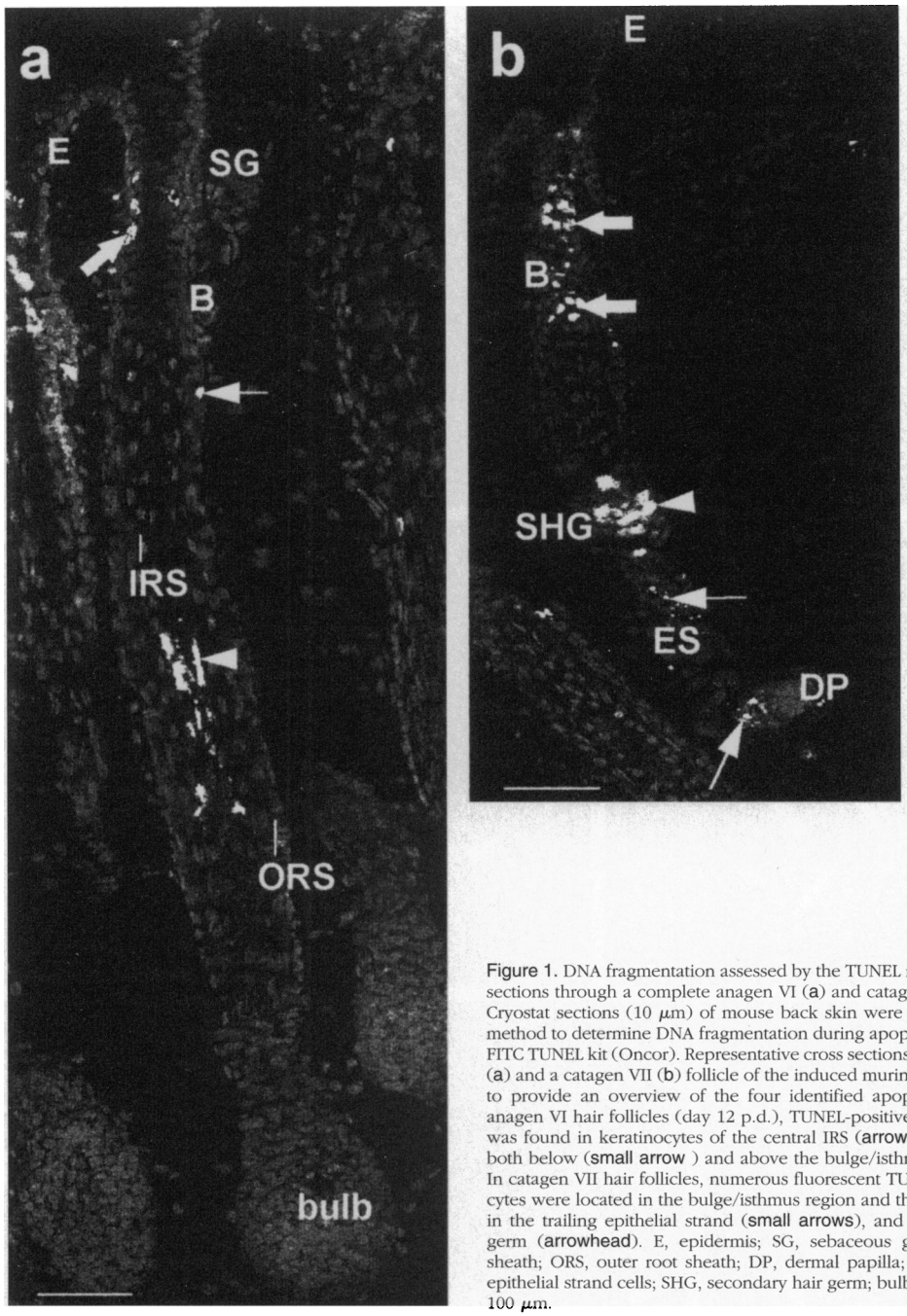

Figure 1. DNA fragmentation assessed by the TUNEL method in longitudinal sections through a complete anagen VI (a) and catagen VII (b) hair follicle. Cryostat sections (10 μm) of mouse back skin were stained by the TUNEL method to determine DNA fragmentation during apoptotic cell death using a FITC TUNEL kit (Oncor). Representative cross sections of an entire anagen VI (a) and a catagen VII (b) follicle of the induced murine hair cycle are shown to provide an overview of the four identified apoptotic hot spots. a: In anagen VI hair follicles (day 12 p.d.), TUNEL-positive staining (bright dots) was found in keratinocytes of the central IRS (arrowhead) and distal ORS, both below (small arrow) and above the bulge/isthmus region (arrow). b: In catagen VII hair follicles, numerous fluorescent TUNEL-positive keratinocytes were located in the bulge/isthmus region and the distal ORS (arrows), in the trailing epithelial strand (small arrows), and in the secondary hair germ (arrowhead). E, epidermis; SG, sebaceous gland; IRS, inner root sheath; ORS, outer root sheath; DP, dermal papilla; B, bulge/isthmus; ES, epithelial strand cells; SHG, secondary hair germ; bulb, hair bulb. Scale bars, 100 μm.

pared with neighboring TUNEL-negative cells). For greater simplicity, TUNEL and Hoechst 33342 double-positive cells, in the following, are referred to as TUNEL positive. TUNEL-positive cells in thymus sections, prepared as positive controls, gave a very similar signal under the same assay conditions, thus attesting to the specificity and sensitivity of the apoptosis demarcation technique used here. In general, only a few isolated TUNEL-positive cells were seen in murine hair follicles during any stage of the anagen VI/catagen/telogen transformation. However, distinct regions of the follicle epithelium displayed clusters of TUNEL-positive cells (apoptosis hot spots) during one or several of the stages described below.

Surprisingly, already in anagen VI (day 12 p.d.), the number of intrafollicular TUNEL-positive cells detectable increased substantially, namely, in the central part of the inner root sheath (IRS) (Figures 1a, 2a, and 3a) and in the distal outer root sheath (ORS), including the isthmus and bulge region (Figures 1a, 2b, and 3a). In late anagen VI (day 16 p.d.) and with the onset of catagen II (day 17 p.d.), the number of TUNEL-positive keratinocytes in the central IRS declined again. Most interestingly, numerous cells in the bulge/isthmus region with epithelial phe-

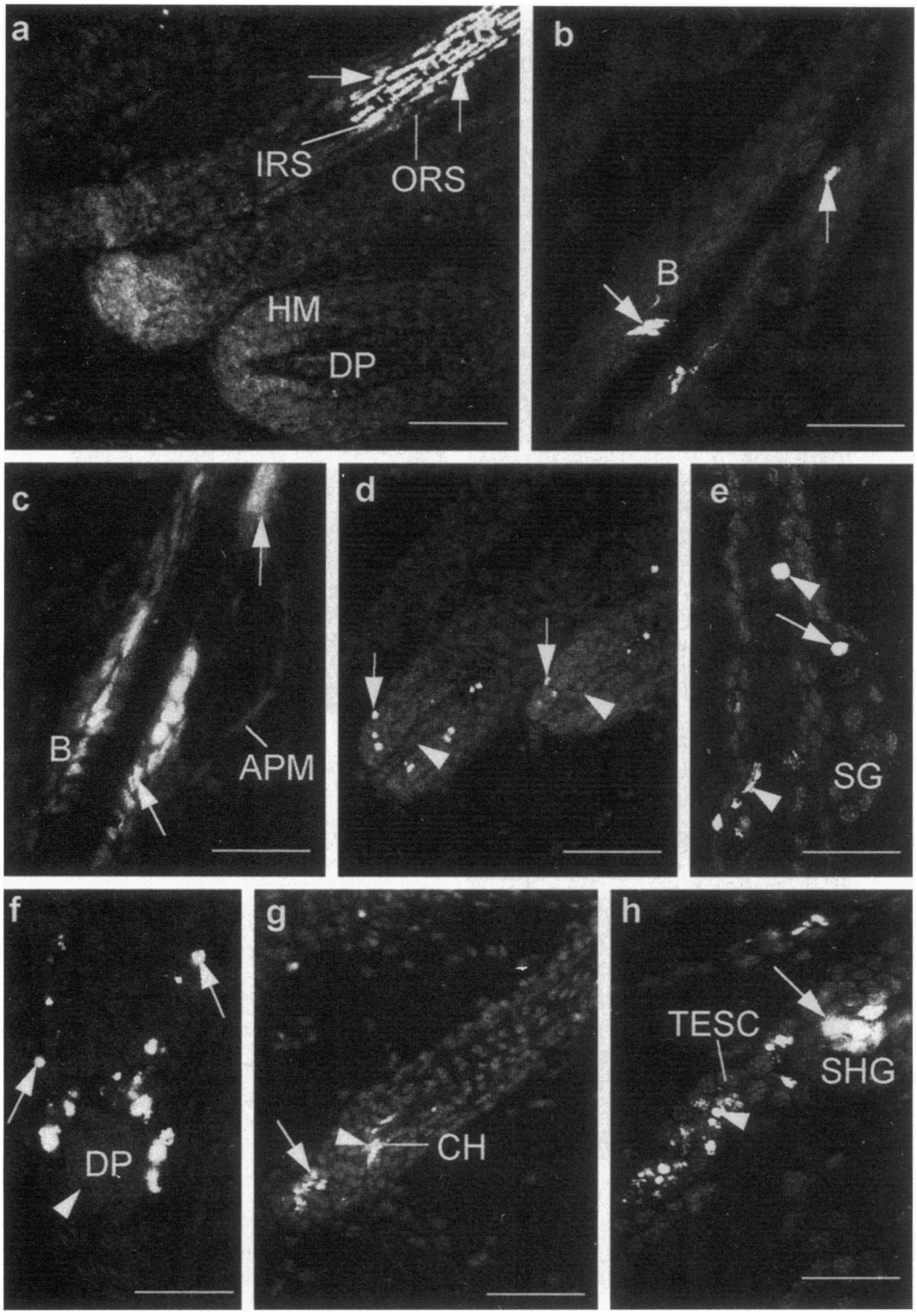

Figure 2. Dynamic patterns of DNA fragmentation assessed by the TUNEL method in keratinocytes during spontaneous hair follicle regression (catagen). Cryostat sections (10 μm) of mouse back skin were stained by a fluorescent modification of the TUNEL method to determine DNA fragmentation during apoptotic cell death in different stages of the induced hair cycle using the FITC TUNEL kit (Oncor). **a** and **b:** In anagen VI hair follicles, TUNEL-positive staining (bright dots) was found in keratinocytes of the central IRS (**a, arrows**) and in the distal ORS beneath and below bulge/isthmus (**b, arrows**). **c:** Surprisingly, in catagen II, cells of the bulge/isthmus region (**arrow**) and cells beneath and below this portion were TUNEL positive. **d:** The first keratinocytes in catagen II, which became TUNEL positive in the proximal region of the hair follicle, were located around the dermal papilla (**arrow**) in the regressing hair matrix. **e:** Isolated TUNEL-positive cells were seen in the sebaceous gland throughout the entire anagen VI catagen development (**arrow**; note also the TUNEL-positive cells in the bulge/isthmus region (**arrowhead**)). **f:** In catagen IV, multiple keratinocytes in the regressing hair matrix around the dermal papilla displayed TUNEL-positive reaction (**arrows**), whereas dermal papilla fibroblasts remained TUNEL negative (**arrowhead**). **g:** Catagen V was associated with TUNEL-positive keratinocytes in the regressing proximal hair bulb (**arrows**) and keratinocytes in close vicinity to the club hair (**arrowhead**). **h:** Numerous strongly fluorescent TUNEL-positive keratinocytes were located in the trailing epithelial strand (**arrowhead**) and the secondary hair germ in catagen VII hair follicles (**arrow**). IRS, inner root sheath; ORS, outer root sheath; HM, hair matrix; DP, dermal papilla; B, bulge/isthmus; CH, club hair; TESC, trailing epithelial strand cells; SHG, secondary hair germ; APM, arrector pili muscle; SG, sebaceous gland. Scale bars, 100 μm (**a, d,** and **g**) and 50 μm (**b, c, e, f,** and **h**).

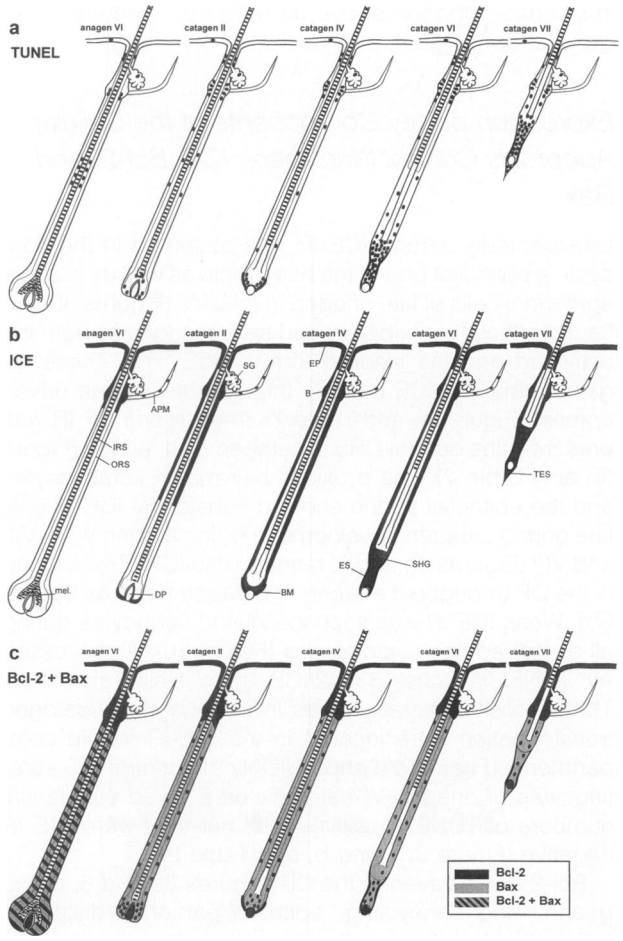

Figure 3. Schematic representation of the topographic distribution of TUNEL-positive cells (**a**), ICE IR (**b**), and Bcl-2/Bax IR (**c**) during different stages of spontaneous hair follicle regression (catagen). Those keratinocytes or hair follicle compartments with TUNEL-positive staining (**a**) or ICE IR (**b**) are in black. Those hair follicle compartments or individual cells with Bcl-2 IR (**c**) and Bax IR are in black and gray, respectively, whereas double-labeled areas or keratinocytes are hatched. The different stages of hair cycle are indicated according to Straile et al [1] with modifications.[18] The summary scheme was derived from analyzing >50 longitudinally sectioned follicles from the lower back of three to five harvested C57BL/6 mice per time point. APM, muscle arrector pili; B, bulge/isthmus; EP, epidermis; ES, epithelial strand; SHG, secondary hair germ; SG, sebaceous gland; ORS, outer root sheath; IRS, inner root sheath; DP, dermal papilla; TES, trailing epithelial strand; meL, melanin.

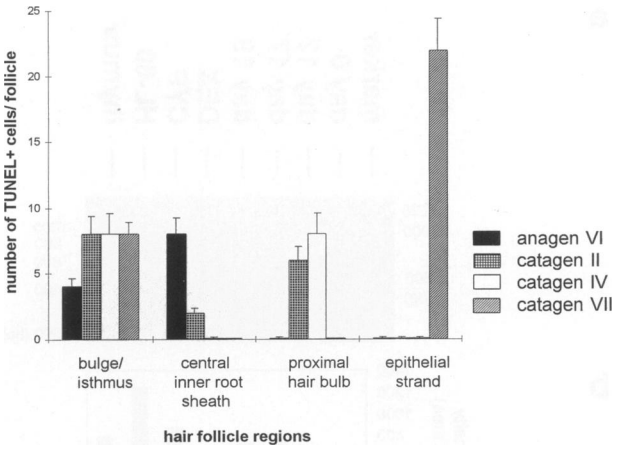

Figure 4. Quantitative histomorphometry of TUNEL-positive cells in the four apoptotic hot spots of the regressing hair follicle at various time points of the anagen-catagen transformation. The number of TUNEL-positive cells/follicle in four different regions (bulge/isthmus, central inner root sheath, proximal hair bulb, and epithelial strand) was counted at four different time points (late anagen VI, catagen II, catagen IV, and catagen VII) of the murine hair cycle. The graph was derived from analyzing >20 longitudinally sectioned follicles from the lower back of three C57BL/6 mice per time point. Note that the epithelial strand does not appear before catagen VI has developed, whereas the proximal hair bulb has been deleted by catagen VII.[1]

notype became TUNEL positive, and throughout catagen development there was a large number of TUNEL-positive cells in this region (Figures 1b, 2c, and 3a). A few keratinocytes just around the dermal papilla (DP) were the first clustered cells of the proximal hair matrix to become TUNEL positive during catagen II (Figures 2d and 3a). The number of TUNEL-positive cells further increased in this region during catagen III, IV, and V (Figures 2, f and g, and 3a). Unexpectedly, even keratinocytes proximal to the differentiating club hair became TUNEL positive in catagen V, VI, and VII (Figures 2g and 3a).

Catagen VI was associated with a very substantial up-regulation of the number of TUNEL-positive keratinocytes in the entire epithelial strand of the involuting hair bulb (Figures 3a and 6, b and c). Notably, cells of the secondary germ also became TUNEL positive at this time (Figures 3a and 6c). In catagen VII and VIII, a strong TUNEL-positive reaction was seen in cells of the epithelial strand as well as in keratinocytes of the residual, regressing ORS (Figures 1b, 2h, and 3a). By quantitative histomorphometry, it became evident that catagen development was associated with a significant ($P < 0.05$) up-regulation of TUNEL-positive cells in the bulge/isthmus and the proximal hair bulb and a down-regulation of TUNEL-positive cells in the central IRS. The number of apoptotic cells in the epithelial strand, which appears only late in catagen development, was by far the highest of any follicle region (Figure 4).

Fibroblasts of the DP were never seen to be TUNEL positive during any of the examined hair cycle stages (Figures 1, a and b; 2, a–d and f; 6b; and 3a). In contrast, isolated sebocytes were TUNEL positive throughout catagen (Figures 2e and 3a).

Endonuclease Activity during Spontaneous and Induced Catagen

It is extremely difficult to demonstrate endonuclease activity, another standard indicator of apoptosis, in an intact, normal organ where only a very small minority of cells at any given time point undergo apoptosis, and the corresponding DNA ladder pattern can at best be expected to yield very faint nucleosome-sized DNA bands.[9] Yet here we provide evidence that DNA laddering can be noted even in normal mouse skin containing hair follicles in various stages of the synchronized anagen- catagen transformation (Figure 5, a and b).

To show the range of oligomeric DNA fragmentation, a marker (500 bp; Boehringer Mannheim, Mannheim, Germany) was used in lane 1 (Figure 5a). To assess endonuclease activity in the different stages of the normal

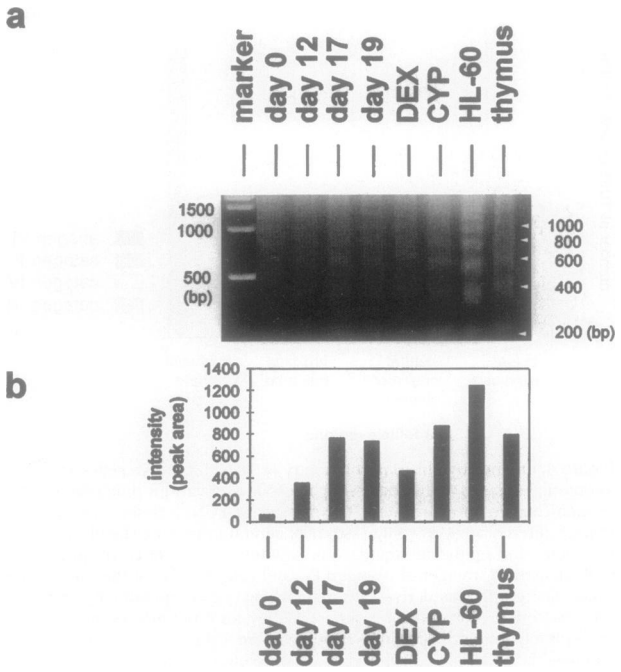

Figure 5. a: Weak DNA laddering of total back skin extracts from various time points of the normal and the pharmacologically manipulated murine hair cycle. DNA fragmentation was visualized using a 2% agarose gel stained with ethidium bromide. To assess endonuclease activity in the different stages of the normal and pharmacologically manipulated murine hair cycle, key time points were selected. In **lane 1**, a 500-bp marker was used. No DNA laddering was seen in telogen skin (day 0 p.d.) (**lane 2**). **Lane 3** showed very weak, ethidium-bromide-stained, fragmented DNA in anagen VI (day 12 p.d). In contrast, DNA extracts of day 17 (**lane 4**) and 19 (**lane 5**) p.d. showed more substantial DNA laddering, represented by oligonucleotides in the range of 180 to 200 bp (**arrowheads**). Dexamethasone-treated skin from day 14 p.d. (**lane 6**) showed DNA fragmentation comparable to normal catagen skin (note that DEX-treated skin samples were taken a few days earlier than normal catagen skin samples) In lane 7, strong ethidium bromide staining was found in skin samples of CYP-treated mice (day 10 p.d.). As positive controls for apoptosis-associated DNA laddering, we used extracted DNA from HL-60 cells in which apoptosis was induced by 1 nmol/L camptothecine (**lane 8**) and from thymus of young mice (**lane 9**). **b:** Densitometric analysis of DNA laddering. The 400-bp band of each lane of the agarose gel was evaluated by computer-assisted densitometry (ScanPack, Biometra).[81]

murine hair cycle, key time points were selected; no DNA laddering was seen in murine back skin with all follicles in telogen (day 0 p.d.; Figure 5, a (lane 2) and b). Very weak ethidium-bromide-stained, fragmented DNA appeared in anagen VI (day 12 p.d.; Figure 5, a (lane 3) and b). In contrast, DNA extracts of days 17 and 19 p.d. showed substantial laddering (Figure 5, a (lanes 4 and 5) and b). Premature, but morphologically normal catagen, which had been induced by DEX, again was less intensive than days 17 and 19 p.d. of spontaneous catagen development (Figure 5, a (lane 6) and b). DNA laddering was most pronounced in skin samples that had been treated with CYP (Figure 5, a (lane 7) and b).

As positive controls for DNA laddering we used HL-60 cells in which apoptosis had been induced by camptothecine[47] (Figure 5a, lane 8) and the thymus of young mice with its high rate of spontaneous thymocyte apoptosis[31,45,46] (Figure 5a, lane 9).

Taken together, this biochemical evidence strongly supports that the TUNEL/Hoechst 33342 double-staining *in situ* data reported above do reflect the occurrence of genuine apoptosis.

Expression of Key Components of the Cellular Apoptosis Control Machinery: ICE, Bcl-2, and Bax

Unexpectedly, strong ICE IR was observed in the noncycling epithelial part of the hair follicle as well as in some epidermal cells of late anagen VI follicles (Figures 3b and 6a; note that the antibody used here recognizes both the activated and the inactive form of ICE[50,51]). These regions remained ICE positive throughout catagen development (Figure 3b and Table 2). In addition, ICE IR was present in the central ORS in catagen II, III, and IV (Figure 3b and Table 2). The proximal hair matrix keratinocytes and the epithelial strand showed substantial ICE IR only late during catagen development, ie, in catagen V, VI, VII, and VIII (Figures 3b and 6, b and c). No ICE IR was found in the DP throughout anagen or catagen (Figures 3b and 6b). Weak ICE IR was seen in isolated sebocytes during all examined hair cycle stages (Figure 3b). As assessed by TUNEL/Hoechst 33342/ICE triple stain, almost all TUNEL-positive keratinocytes in the anagen VI/catagen transformation were located in the ICE-IR follicle compartments (Figure 3, a and b). Only the central IRS keratinocytes of anagen VI hair follicles showed substantial numbers of TUNEL-positive cells, but they were ICE IR negative (Figure 3, a and b, and Table 2).

Bcl-2 IR was seen in the DP (Figures 3c and 6, d and g) and in the "noncycling," epithelial part of the distal hair follicle (Figures 3c and 6, d and g) during all examined cycle stages. Keratinocytes of the bulge and isthmus region were only Bcl-2 positive and Bax negative (Figures 3c and 6e), whereas cells in the proximal IRS, ORS, and hair matrix in late anagen VI displayed both Bcl-2 and Bax IR (Figures 3c and 6f). Only in the epidermis, DP, and distal ORS (including the bulge/isthmus region) did Bcl-2 remain strongly expressed throughout catagen development, and no Bax IR was seen in these regions (Figures 3c and 6e and Table 2). Double immunovisualization of Bcl-2/Bax IR showed a sudden, progressive decline of Bcl-2 IR, associated with a simultaneous increase of Bax IR in proximal hair matrix keratinocytes during catagen II to VIII, compared with that in anagen VI (Figures 3c and 6g). In catagen II, Bcl-2-IR keratinocytes were still present in the regressing hair matrix (Figure 3c), but by catagen VI, practically all keratinocytes in the epithelial strand showed a strong predominance of Bax IR, and only a few isolated epithelial cells in the secondary hair germ (SHG) were Bcl-2/Bax double positive (Figures 3c and 6g). No Bax IR was found in DP fibroblasts in any of the studied anagen or catagen stages (Figures 3c and 6g).

In summary, almost all follicle regions below the bulge/isthmus region, where the majority of apoptotic cells was located during catagen development, were also strongly Bax and ICE positive, and a sudden decline in Bcl-2 IR coincided with the onset of apoptosis below the level of the bulge/isthmus. However, even in the permanently

Bcl-2-positive distal ORS, clusters of TUNEL-positive cells became visible throughout catagen, accompanied by strong, homogeneous expression of ICE IR in this region.

Expression of Apoptosis-Associated Receptors Fas/Apo-1, p55^{TNFR}, and p75^{NTR}

In anagen VI hair follicles, Fas/Apo-1 was expressed on individual keratinocytes in the central ORS, and its expression was homogeneously distributed within the bulge/isthmus region (Figures 6h and 7a), where Fas IR was seen throughout the anagen-catagen-telogen transformation. Keratinocytes of the proximal ORS, IRS, and hair matrix were Fas/Apo-1 negative in anagen VI follicles. In catagen II, only individual keratinocytes in the proximal and central portions of the ORS showed Fas/Apo-1 IR, whereas practically all keratinocytes in the bulge/isthmus were Fas/Apo-1 positive (Figure 7a and Table 2). During further catagen development, expression of Fas/Apo-1 was found in the entire central ORS (catagen IV to VI) and individual Fas/Apo-1-IR keratinocytes appeared in the regressing epithelial strand, the secondary hair germ, and the central IRS (Figure 6i). DP fibroblasts did not display any Fas/Apo-1 IR during the entire anagen-catagen transformation.

Strong p75^{NTR} IR expression was noted only in the central ORS and in the distal portion of the proximal ORS between anagen VI (Figures 6j and 7b) and catagen IV. In addition, this receptor was expressed in the isthmus and bulge region during catagen II to VIII (Figure 6k) and in the regressing epithelial strand as well as the secondary hair germ during catagen VI to VIII (Figures 6l and 7b). Interestingly, neither Fas/Apo-1 nor p55^{TNFR-} or p75^{NTR} IR could be detected in DP fibroblasts during any of the anagen-catagen-telogen transformation stages of the hair follicle (Figures 6, i, l, and m, and 7).

The two different antibodies used to detect the TNF receptor type I antigen (Table 1, a and b), showed almost the same IR pattern. In contrast to the more restricted expression patterns of Fas/Apo-1 and p75^{NTR}, p55^{TNFR} was very widely expressed in anagen VI follicles (Figure 7c); p55^{TNFR} IR was seen in the proximal ORS and IRS (Figures 6m and 7c), and relatively weaker expression was seen in the central and distal ORS and the isthmus/bulge region (Figure 7c and Table 2). In catagen II, the area of strong follicular p55^{TNFR} IR expression increased dramatically, and enhanced p55^{TNFR} IR was seen not only in the proximal ORS but also in the central portion of the hair follicle ORS (Figures 6n and 7c). During catagen IV to VII, strong p55^{TNFR} IR was observed in the proximal and central ORS and in the regressing epithelial strand (Figures 6o and 7c). Relatively weak expression of this receptor remained visible in the isthmus/bulge region throughout catagen development, and no p55^{TNFR} IR was found in the DP during any hair cycle stage (Figures 6m and 7c).

To summarize, the noncycling distal follicle epithelium expressed Fas, p55^{TNFR}, and p75^{NTR} throughout the hair cycle (with hardly any changes in IR throughout catagen development), whereas distinct regions of the regressing portion of the hair follicle showed a differential up-regulation of these apoptosis-associated receptors. In early catagen, only p55^{TNFR} was expressed in hair matrix keratinocytes, whereas Fas/Apo-1 and p75^{NTR} expression was restricted to the ORS. In late catagen, all three receptors were found in the regressing central ORS, the epithelial strand, and the secondary hair germ, whereas the central IRS showed only Fas/Apo-1 IR (see Figure 7 and Table 2).

Pharmacologically Manipulated Hair Follicle Regression

The treatment of anagen VI follicles *in vivo* with DEX or CYP, which terminates anagen VI and induces massive, premature catagen development,[27,39] induced striking changes in their expression of apoptosis-related parameters, and pharmacologically manipulated catagen displayed several interesting differences in the number of TUNEL-positive cells and in ICE, Bcl-2, Bax, Fas/Apo-1, p55^{TNFR}, and p75^{NTR} IR, compared with spontaneous catagen development (Table 3).

After DEX treatment, the number of TUNEL-positive keratinocytes in the regressing hair matrix was not substantially increased compared with the normal anagen VI/catagen transformation (compare Figures 2d and 8a and Table 3). As during normal hair follicle cycling, DP fibroblasts were never TUNEL positive in the skin of DEX- or vehicle-treated mice (Figure 8a). CYP-induced precocious catagen, in contrast, which is characterized by the development of severe hair follicle dystrophy and alopecia,[39,41] displayed a massive increase in the number of TUNEL-positive cells throughout the entire proximal ORS, IRS, and hair matrix (Figure 8b).

A strong up-regulation of constitutive ICE IR was found in the regressing portion of the hair follicle epithelium, both in DEX-induced (Figure 8a) and CYP-induced (Figure 8c) catagen (compared with anagen VI and with normal catagen development (Table 3). Interestingly, compared with spontaneous catagen development, both DEX- and CYP-induced catagen were associated with a strong up-regulation of Bax IR in the entire proximal hair follicle epithelium and in DP fibroblasts, whereas Bcl-2 became undetectable in this region (Figure 8, d and e). Both forms of pharmacologically manipulated catagen showed increased Fas/Apo-1 IR in the entire central ORS compared with spontaneous catagen (cf Figure 7a), whereas the other follicle regions did not differ substantially in their Fas/Apo-1 expression from vehicle-treated anagen VI follicles or from spontaneous catagen follicles (Table 3). p55^{TNFR} IR in the proximal ORS and IRS (Figure 8g) was enhanced by CYP and DEX, compared with normal catagen development. Major differences between CYP- and DEX-induced catagen were observed in the patterns of p75^{NTR} IR, which was present in DP fibroblasts only after CYP, but not after DEX, treatment (Figure 8h). Thus, the two forms of pharmacological catagen manipulation differed mainly in their effect on follicle ke-

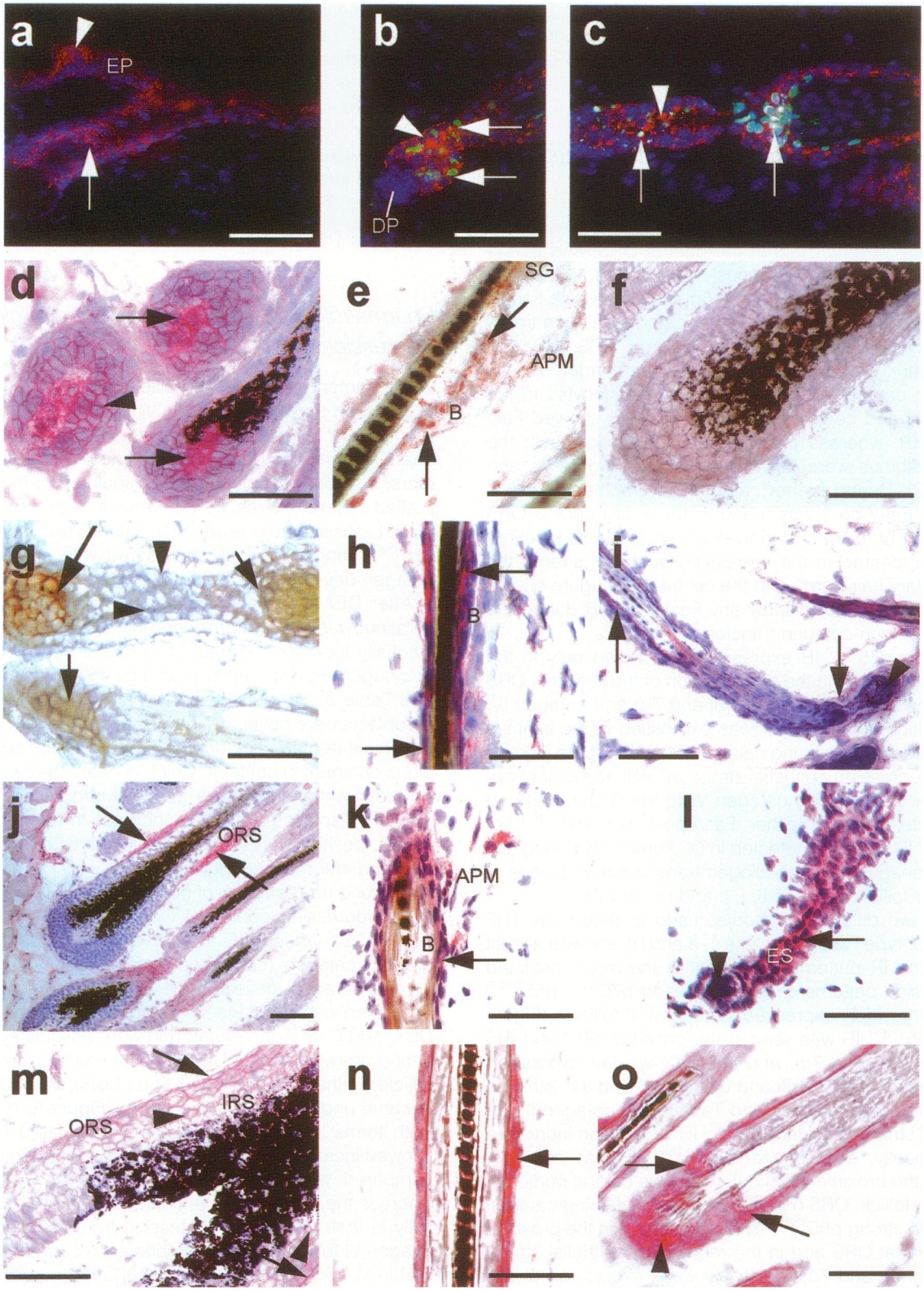

Figure 6. Expression of different apoptosis-associated markers and receptors during the spontaneous anagen-catagen transformation. Cryostat sections (10 μm) of mouse skin were stained by various antisera. **a:** ICE IR (red fluorescence, **arrowhead**) was seen in the epidermis and the distal hair follicle ORS (including the bulge/isthmus region, **arrow**) in anagen VI. Counterstaining of cell nuclei was done by Hoechst 33342 (blue fluorescence; also in Figure 6, b and c). **b:** In catagen V ICE IR (red, **arrowhead**) was seen in the epithelial strand, where simultaneously multiple TUNEL-positive cells (green fluorescence, **arrows**) were located. DP fibroblasts were TUNEL and ICE negative (DP). **c:** Catagen VI hair follicles showed ICE IR (red) in the proximal ORS, the epithelial strand (**arrowhead**) and secondary hair germ. In these regions TUNEL-positive cell fragments (**small arrow**) and intact cells (**large arrows**) were located. **d:** Bcl-2 IR (red) was shown in the dermal papilla (**arrows**) and hair matrix (**arrowhead**) in anagen VI. As in the following panels (except **e**, **f**, and **g**), counterstaining was performed with Meyer's hemalaun (blue). **e:** Cells of the bulge/isthmus region in anagen VI were visualized by Bcl-2/Bax double-staining but showed only Bcl-2 IR (red, **arrows**). **f:**

Table 2. Comparison of the Expression Patterns of Various Apoptosis-Related Parameters during the Spontaneous Anagen-Catagen Transformation

	Anagen VI	Catagen II	Catagen III	Catagen IV	Catagen V	Catagen VI	Catagen VII	Catagen VIII
TUNEL/ Hoechst 33342	c IRS, **d ORS**	**B**, c IRS, d/c ORS, **p HM**	B, d/c ORS, p HM	B, d/c/**p ORS,** p HM	B, d/c/p ORS, p HM, **CH**	B, d/c/p ORS, CH, **ES, SHG**	B, d/p ORS, ES	B, ES
ICE	SG, EP, d ORS, B,	SG, EP, B, **d/c ORS, HM**	SG, EP, B, d/c ORS, HM,	SG, EP, B, d/c/p ORS, HM	SG, EP, B, d/c/p ORS, HM, **ES**	SG, EP, B, d/c/p ORS, ES, **SHG**	SG, EP, B, d/c/p ORS, ES, SHG	SG, EP, B, d/c/p ORS, ES, SHG
Bcl-2	EP, B, IRS, HM ORS, DP	EP, B, HM, ORS, DP	EP, B, HM, ORS, DP	EP, B, HM, ORS, DP	EP, B, ORS, DP	EP, B, DP, ORS, **SHG**	EP, B, DP, ORS, SHG	EP, B, DP, ORS, SHG
Bax	c/p ORS, IRS, HM	c/p ORS, IRS, HM	c/p ORS, IRS, HM	c/p ORS, IRS, HM	c/p ORS, IRS, HM, SHG	c/p ORS, IRS, ES, SHG	ORS, IRS, ES, SHG	ORS, ES, SHG
Fas/Apo-1	B, d and p portion of c ORS,	B, **c/p ORS**	B, c/p ORS	B, c/p ORS	B, c/p ORS	B, c/p ORS, **ES, c IRS, SHG**	B, SHG	ORS, SHG
$p75^{NTR}$	B, c/p ORS	B, c/p ORS	B, c/p ORS	B, c/p ORS	B, c/p ORS	B, c/p ORS, **ES, SHG**	B, ORS, ES, SHG	B, ORS, SHG
$p55^{TNFR}$	EP, B, d/c/p ORS, p IRS	EP, B, d/c/p ORS, **HM**	EP, B, d/c/p ORS, HM	EP, B d/c/p ORS, HM	EP, B, d/c/p ORS, HM	EP, B, d/c/p ORS, **ES, SHG**	EP, B, ORS, ES, SHG	EP, B, ORS, SHG

EP, epidermis; ES, epithelial strand; SHG, secondary hair germ; HM, hair matrix; CH, club hair; p, proximal; d, distal; c, central; B, isthmus/bulge region. Bold print indicates changing expression pattern in comparison with the stage described before.

ratinocyte apoptosis and on $p75^{NTR}$ expression by DP fibroblasts.

Discussion

Using a combined TUNEL/Hoechst 33342 staining technique (Figures 1, 2, 6, b and c, and 8, a and b), this study complements and supports existing ultrastructural evidence that keratinocyte apoptosis does occur during normal[2,3] as well as during pathological[42,53] and experimentally induced hair follicle regression.[16,17,43,54,55] We also provide biochemical evidence that both spontaneous and pharmacologically manipulated catagen are associated with endonuclease activation (Figure 5, a and b). Furthermore, we identify previously unrecognized hot spots of intrafollicular apoptosis and show that physiological and pathological catagen are characterized by an up-regulation of ICE expression and an apparent inversion of the Bcl-2/Bax ratio in all epithelial follicle regions that undergo involution during catagen (Figure 3 and Tables 2 and 3).

The current study has generated the first "apoptomap" of the murine hair follicle during spontaneous and induced regression. It provides a detailed chart on the time course and exact localization of intrafollicular apoptosis during the anagen-catagen transformation and its spatiotemporal correlation with the expression of key intracellular and cell surface parameters implicated in apoptosis control (ICE, Bcl-2, Bax, Fas, $p75^{NTR}$, and $p55^{TNFR}$). This chart will become even more useful when it is systematically complemented by other researchers in the field. Such complementary studies should include an analysis of additional components of the apoptosis control machinery (eg, other members of the TNF/NGF receptor, Bcl-2, and ICE-like protease families and FADD and transglutaminases) and of the status of the cell cycle machine of those keratinocytes destined to undergo apoptosis (namely their c-*myc*, c-*fos*, p53, p35, and p21 expression) as well as elucidation of the intrafollicular expression patterns of Fas ligand, neurotrophins, and TNF-α (cf Refs. 4, 5, 10, 30, 34, 36, and 56). (The schematized, computer-generated drawings of the murine hair follicle in defined transformation stages used in the present study can be requested from the authors so as to promote standardized recording techniques and data presentation for hair research in the murine system.)

Our apoptomap (Figures 3 and 7) allows one to pharmacologically target the parameters studied here much

Anagen VI keratinocytes in the proximal hair matrix were double stained as in Figure 6e and expressed both Bcl-2 (red-brown color) and Bax IR (blue color). **g:** In catagen VI, Bcl-2 IR was found in the dermal papilla (**large arrow**) and keratinocytes of the secondary hair germ (**small arrow**), whereas a predominance of Bax over Bcl-2 IR was seen in the regressing epithelial strand (**arrowheads**). **h:** Fas/Apo-1 IR (red) was found in the bulge/isthmus (**arrows**) and in the distal portion of the central ORS in anagen VI. The same pattern was seen throughout catagen development. **i:** In catagen VI, slightly Fas/Apo-1-IR keratinocytes were found in the proximal ORS and the regressing epithelial strand (**arrows**), whereas the dermal papilla was Fas/Apo-1 negative (**arrowhead**). **j:** The proximal and central ORS displayed $p75^{NTR}$ IR (red, **arrows**) during anagen VI. **k:** In catagen II, $p75^{NTR}$ expression was found in the bulge/isthmus (red, **arrow**). **l:** In catagen VI, the regressing epithelial strand showed $p75^{NTR}$ IR (red, **arrow**), whereas dermal papilla fibroblasts were $p75^{NTR}$ negative (**arrowhead**). **m:** $p55^{TNFR}$-IR (red) was expressed in the proximal ORS (**arrows**) and IRS (**arrowheads**) in anagen VI. **n:** Keratinocytes of the central ORS were $p55^{-TNFR}$ during catagen II (**arrows**). **o:** During catagen VI, cells located in the secondary hair germ (**arrowhead**), regressing proximal ORS (**arrows**), and distal ORS were $p55^{TNFR}$ IR (red). B, bulge/isthmus; EP, epidermis; ES, epithelial strand; SG, sebaceous gland; SHG, secondary hair germ; ORS, outer root sheath; IRS, inner root sheath; DP, dermal papilla; APM, arrector pili muscle. Scale bars, 50 μm (all except j) and 100 μm (j).

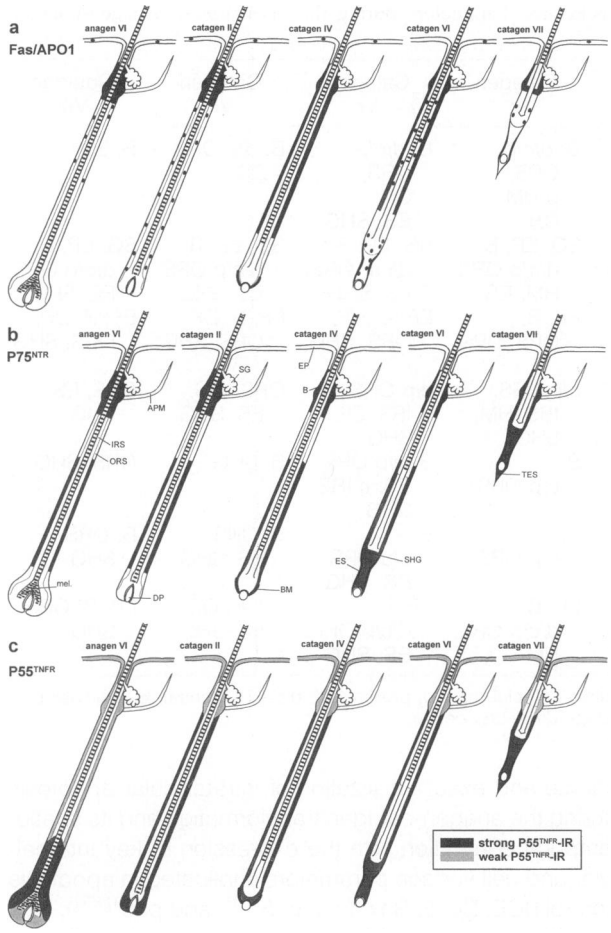

Figure 7. Schematic representation of the topographic distribution of apoptosis-associated receptor (Fas/Apo-1 IR (**a**), $p75^{NTR}$ IR (**b**), and $p55^{TNFR}$ IR (**c**)) expression during different stages of spontaneous hair follicle regression. Those keratinocytes or hair follicle compartments with strong Fas/Apo-1 IR (**a**), $p75^{NTR}$ IR (**b**), or $p55^{TNFR}$ IR (**c** are shown in dark gray. Hair follicle compartments that displayed weak $p55^{TNFR}$ IR are shown in light gray (**c**). The different stages of the hair cycle are indicated according to Straile et al[1] with some modifications.[18] The summary scheme was derived from analyzing >50 longitudinally sectioned follicles from the lower back of three to five C57BL/6 mice harvested per time point for every antigen. APM, arrector pili muscle; B, bulge/isthmus; EP, epidermis; ES, epithelial strand; SG, sebaceous gland; SHG, secondary hair germ; ORS, outer root sheath; IRS, inner root sheath; DP, dermal papilla; TES, trailing epithelial strand.

more selectively than previously possible, so as to modulate keratinocyte apoptosis in the follicle (and thus catagen development) with improved efficiency. For example, agonists and antagonists of $p55^{TNFR}$ or $p75^{NTR}$ can now be administered, knowing when and where in the follicle maximal receptor expression promises maximal stimulation responses. As the majority of hair growth disorders seen in clinical practice largely reflects premature or retarded catagen development,[18] this apoptomap should assist in the development of reliable and effective catagen-modulatory drugs. For example, inhibitors of ICE-like cysteine proteases, of endonuclease activity, and of $p75^{NTR}$-mediated signal transduction as well as agents that up-regulate Bcl-2 expression in the hair bulb promise to be effective catagen-blocking agents for the treatment of telogen effluvium or chemotherapy-induced alopecia.[4,18] To be truly useful in a routine clinical setting, such agents would have to be topically effective. This may be achieved by the use of follicle-targeted liposome preparations (cf Refs. 57 to 59).

The apoptomap reported here contradicts conventional hair research concepts in several respects. Most notably, it reveals that keratinocyte apoptosis in normal murine hair follicles commences much earlier than previously appreciated and occurs not only in the regressing proximal hair bulb but also in three additional hot spots of intrafollicular apoptosis. Already during mid-anagen VI (day 12 p.d.), ie, long before the regression of anagen follicles becomes morphologically noticeable, dense clusters of apoptotic keratinocytes are seen in the central IRS and in the distal ORS (Figures 1, 2, a and b, and 3a), and throughout catagen development, there is prominent apoptosis not only in the proximal ORS but also in its most distal quarter (Figure 3a). The third apoptosis hot spot is located in the secondary hair germ of advanced catagen follicles (Figure 6c), where ultrastructural studies had not detected signs of keratinocyte apoptosis.[2,3] Possibly, the apoptosis clusters seen in the central IRS of mid-anagen VI follicles serve to maintain the IRS at a constant length by deleting surplus IRS cells. During catagen, the simultaneous deletion of keratinocytes in four distinct apopto-

Table 3. Pharmacologically Manipulated Catagen: Comparative Summary of Expression Patterns of Apoptosis-Related Parameters

	Differences to vehicle-treated anagen VI/spontaneous catagen development	
	DEX	CYP
Number of TUNEL+ cells	–	Entire ORS, IRS, and HM
		↑ ↑ ↑
ICE	Entire central and proximal HF	Entire central and proximal HF
	↑ ↑ ↑	↑ ↑ ↑
Bcl-2	ORS, IRS, HM, and DP	ORS, IRS, HM, and DP
	↓ ↓ ↓	↓ ↓ ↓
Bax	ORS, IRS, HM and DP	ORS, IRS, HM, and DP
	↑ ↑ ↑	↑ ↑ ↑
Fas/Apo-1	Central ORS	Central ORS
	↑	↑
$p75^{NTR}$	–	DP
		↑ ↑ ↑
$p55^{TNFR}$	ORS, IRS, and HM	ORS, IRS, and HM
	↑ ↑	↑ ↑

HM, hair matrix; HF, hair follicle; ↑, ↑ ↑, and ↑ ↑ ↑, weak, strong, and very strong up-regulation; ↓, ↓ ↓, and ↓ ↓ ↓, weak, strong, and very strong down-regulation; –, no substantial differences.

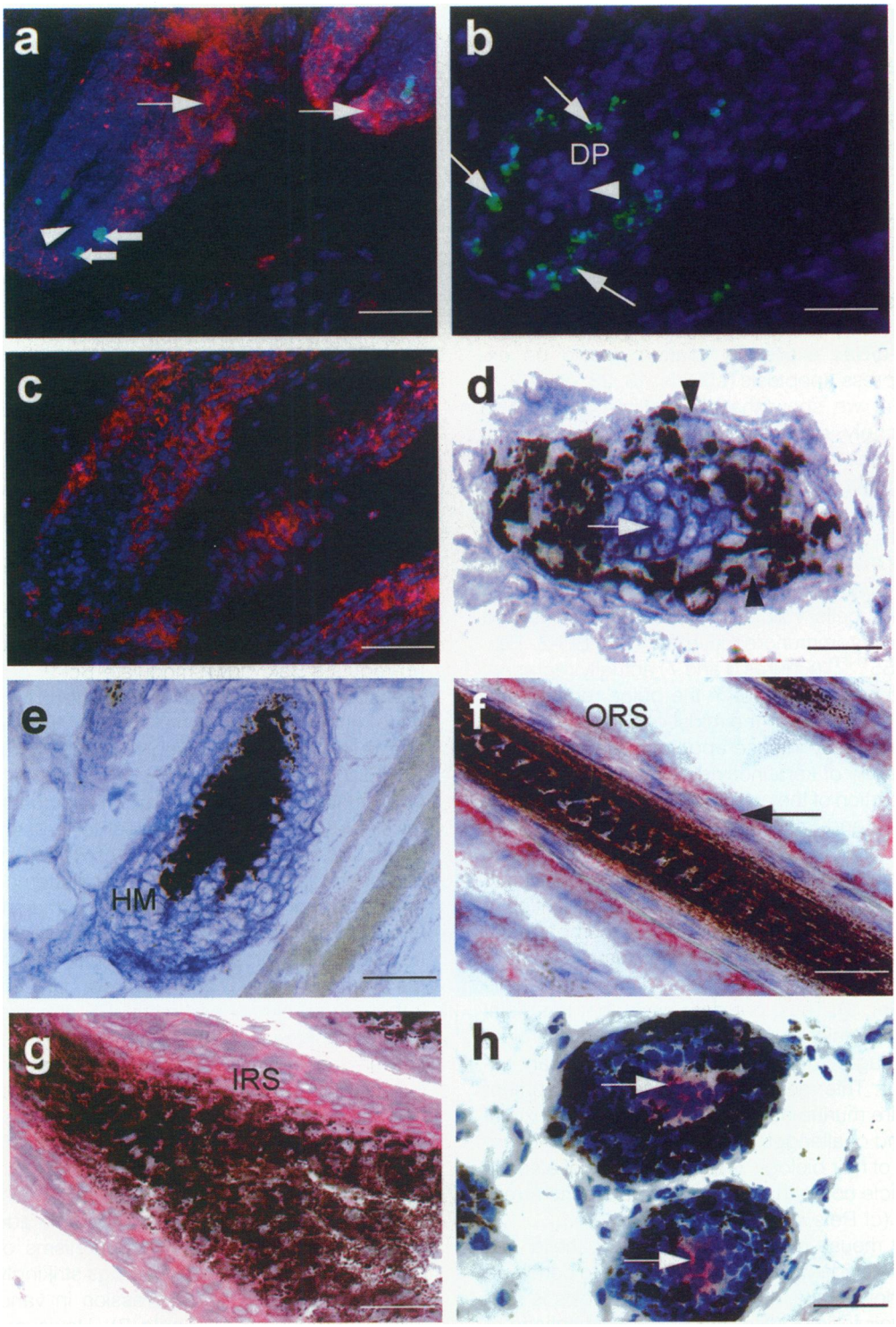

Figure 8. Distribution of apoptosis-associated markers and receptors in hair follicles during pharmacologically manipulated catagen. Cryostat sections (10 μm) of DEX- or CYP-treated mouse skin were stained by the TUNEL method (**a** and **b**, green fluorescence), and in addition, immunovisualization of ICE IR was performed (**a**, red fluorescence), whereas in **c** only ICE IR was detected. Sections were counterstained by Hoechst 33342 (**a** to **c**, blue fluorescence). Double immunovisualization of Bcl-2/Bax IR was done in **d** and **e**, whereas single immunodetection of Fas/Apo-1 (**f**), $p55^{TNFR}$ (**g**), and $p75^{NTR}$ IR (**h**) was performed. **a:** Catagen II hair follicles after DEX treatment display only a few isolated TUNEL-positive (**small arrows**) but strong ICE IR (**large arrow**) keratinocytes in proximal hair matrix. Dermal papilla (DP) fibroblasts remained TUNEL and ICE negative. **b:** After CYP treatment, numerous TUNEL-positive hair matrix keratinocytes were seen (**arrows**), but DP fibroblasts were always TUNEL negative (**arrowheads**). **c:** Dramatic increase of ICE IR in the entire regressing portion of the hair follicle (proximal hair matrix, central IRS, and ORS) was observed in CYP-treated skin (red fluorescence). **d:** After CYP, upregulation of Bax (blue) and absence of Bcl-2 IR (red-brown) were found in the proximal hair bulb (**arrowheads**) and particularly in the DP (**arrow**); ectopic melanin granules can be seen as a sign of follicle dystrophy[39,41]. **e:** After DEX treatment, keratinocytes of the proximal hair matrix were only Bax positive (blue staining) and Bcl-2 negative (note the absence of a red-brown color reaction). **f:** Dexamethasone-treated skin showed an upregulation of Fas/Apo-1 IR (red) in the central ORS (**arrow**). **g:** $p55^{TNFR}$ IR in the proximal ORS and IRS was extremely pronounced in anagen VI hair follicles. **h:** Strong $p75^{NTR}$ IR appeared in DP fibroblasts of dystrophic catagen II follicles after CYP treatment (**arrows**; note again the ectopic melanin granules). ORS, outer root sheath; IRS, inner root sheath; DP, dermal papilla; HM, hair matrix. Scale bars, 50 μm (except **c**) and 10 μm (**c**).

sis hot spots may explain the amazing speed of murine hair follicle involution, during which the follicle shortens its length between anagen VI and telogen by more than two-thirds within approximately 2 days.[1,27]

As the bulge region of the ORS harbors a major epithelial stem cell population, the progeny of which probably generates a new anagen hair bulb after catagen and telogen have been traversed,[60] it is quite unexpected that this region should be a hot spot of keratinocyte apoptosis during catagen. This is the more surprising as the distal ORS (including the isthmus/bulge region) prominently expresses Bcl-2 throughout catagen development (as shown before[61]) and hardly any Bax (Figures 3c and 6e). This Bcl-2/Bax expression pattern would be expected to suppress apoptosis (cf Refs. 13, 23, and 62) in this region. Yet we show that this follicle region also expresses strongly, rather homogeneously, and consistently ICE and the apoptosis receptors Fas/Apo-1 and $p75^{NTR}$ throughout the entire anagen-catagen transformation (Figures 3b; 6, h and k; and 7, a and b). Thus, the majority of cells in the distal ORS is equipped with key components of the molecular machinery for inducing programmed cell death. It now needs to be identified which of the apoptotic cells visible in the bulge/isthmus and which of the cells immunoreactive for ICE, Bcl-2, Fas, $p75^{NTR}$, and $p55^{TNFR}$ (Figures 3 and 7) actually represent stem cells and how stem cells in the bulge region manage to escape cell death in the midst of a tissue environment characterized by intense apoptotic activity.

The prominence of keratinocyte apoptosis in the ORS distal to the insertion of the arrector pili muscle (Figures 1, a and b; 2, b–c; and 3a) also reveals that this so-called noncycling hair follicle segment is not as permanent as traditionally assumed (cf Refs. 18, 19, 60, and 63). Due to the velocity of programmed cell death, the visualization of even a few apoptotic cells within a tissue compartment indicates that actually much more apoptosis occurs here than the mere number of demarcated apoptotic cells suggests (cf Ref. 9). Thus, our data imply that the distal follicle epithelium deletes a substantial percentage of its cells during catagen, thereby undergoing significant tissue remodeling. This means that catagen development affects the entire murine hair follicle, not only its proximal component, and challenges the validity of a much-loved, basic concept of hair biology, ie, the existence of a small, permanent follicle compartment located above the arrector pili muscle (cf Refs. 18, 19, 60, 63, and 64).

The present mouse model for studying epithelial cell apoptosis *in vivo* evidently does not allow one to conclude with certainty how exactly keratinocyte apoptosis is regulated in the hair follicle. Also, the obvious limitations of immunohistological data prevent that more than first pointers to the up- and downstream molecular controls of follicle keratinocyte apoptosis can be distilled from the current study. Yet the IR patterns summarized in this apoptomap of the murine hair follicle (Figures 3 and 7) provide several interesting clues.

Our study supports that the downstream controls of follicle keratinocyte apoptosis follow one of the most widely used, evolutionarily most highly conserved scenarios demonstrated, eg, for nematodes, thymocytes, mature T and B lymphocytes, neurons, and many hormone-dependent epithelial cells *in vivo* and *in vitro* (cf Refs. 10, 65, and 66). Other than Bcl-2/Bax- and/or endonuclease-independent forms of apoptosis described for various cell systems and experimental conditions (cf Ref. 13), follicular keratinocyte apoptosis in health and disease seems to involve a sudden decline in the Bcl-2/Bax ratio, followed by ICE activation and, finally, endonuclease activation (cf Refs. 12, 23, and 30).

This hypothesis can be probed by repeating the same assays as the ones reported here in appropriate mouse mutants and their wild-type littermates (studying, eg, Bcl-2 knockout[67] or Bcl-2-overexpressing transgenic mice[68]). If this hypothesis is correct, the administration of known endonuclease or ICE inhibitors to murine anagen follicles *in vivo* should retard catagen and should inhibit chemotherapy-induced follicle keratinocyte apoptosis, catagen, and/or alopecia. Preliminary evidence suggests indeed that the oral administration of Zn^{2+}, which inhibits endonuclease activity,[69,70] does exert these predicted effects.[71]

In principal, molecular targets for the development of novel hair drugs may include topically administered caspase or endonuclease inhibitors for the management of unwanted hair loss and topical agents that selectively up-regulate Bax, down-modulate Bcl-2, or activate ICE-like proteases or endonuclease in follicle keratinocytes so as to remove unwanted hair growth. However, our study has revealed disappointingly little correlation between TUNEL-positive cells and the expression of standard apoptosis-associated molecules, which questions whether follicle keratinocytes are subject to the same apoptosis control as other keratinocytes (cf Ref. 72). Also, until it has been clarified whether similar patterns of apoptosis and its control occur in murine and human hair follicles, it is premature to predict the effects of manipulating intrafollicular apoptosis on human hair growth. For example, Tamada et al[73] have reported TUNEL-positive cells in both the proximal and distal IRS of human anagen VI follicles, whereas we have detected TUNEL-positive cells only in the central IRS of murine anagen VI follicles. Furthermore, there are recognized differences in club hair shedding between men and mice, which may reflect species-dependent differences in apoptosis-driven follicle regression and club hair shedding.

The results of pharmacological catagen manipulation by topical DEX or systemic CYP provide additional hints. Despite their very different mechanisms of action and routes of administration, both drugs strikingly up-regulate ICE, Bax, and $p55^{TNFR}$ expression in various epithelial follicle compartments (Table 3). However, only in the case of CYP is this also associated with a massive up-regulation of keratinocyte apoptosis in anagen VI and catagen follicles (Table 3 and Figure 8b). This suggests that the up-regulation of ICE, Bax, and $p55^{TNFR}$ expression alone does not suffice to trigger follicle keratinocyte apoptosis. Likewise, even the stimulation of $p75^{NTR}$ expression by CYP in the normally $p75^{NTR}$-negative DP as well as the up-regulation of Bax and the suppression of Bcl-2 IR by CYP here fail to trigger apoptosis in this highly specialized fibroblast population, which never expresses

ICE and Fas IR (Figure 4). Taken together, these "apoptomap" characteristics of DP fibroblasts may explain in part why follicles are so comparatively resistant to irreversible, permanent damage by chemotherapy (cf Refs. 39 and 40).

Concerning the upstream controls of normal follicle keratinocyte apoptosis, the IR patterns characterized here render it unlikely that Fas or $p55^{TNFR}$ play critical roles in triggering the apoptosis of follicle keratinocytes in the proximal hair bulb during spontaneous catagen. As demonstrated by TUNEL/Hoechst 33342 stain, early during follicle regression, the proximal hair bulb becomes the most prominent site of intrafollicular apoptosis (Figures 2d and 3a), and throughout catagen most apoptotic cells are seen in the regressing hair bulb (Figures 1b; 2, d and f–h; 3a; and 6, b and c). Yet neither Fas nor $p55^{TNFR}$ display substantially increased levels of expression in this region during early catagen (Figures 6i and 7, a and c, and Table 2). In fact, Fas is most prominently expressed in the nonregressing, distal follicle epithelium (Figures 6h and 7a), where it may well be involved in the control of apoptosis induction. The striking expression of p55TNFR around the club hair in late catagen development (Figure 6o) raises the question whether p55TNFR stimulation is involved in club hair formation. In the regressing hair follicle, instead, the rather weak Fas expression, which is seen on only relatively few cells (Figures 6i and 7a), argues against Fas as an important factor in controlling keratinocyte apoptosis. The same may be true for $p55^{TNFR}$, as its expression in the hair bulb remains fairly constant throughout the anagen-catagen transformation, is strongly expressed in the nonapoptotic anagen hair bulb, and even disappears from the regressing proximal IRS despite its rapid involution (Figure 7c).

In contrast, an up-regulation of $p75^{NTR}$ expression is seen in those regions of the proximal follicle epithelium where the most dramatic keratinocyte apoptosis occurs, and this around the time period when the number of apoptotic cells increases (compare Figures 3a; 6, c and l; and 7b). Also, throughout the anagen-catagen transformation, $p75^{NTR}$ expression is consistently high in the distal ORS, one of the apoptosis hot spots of the murine hair follicle (Figures 3a and 7b). Thus, particularly in the hair bulb, $p75^{NTR}$ expression might be more intimately involved in controlling follicle keratinocyte apoptosis than Fas and $p55^{TNFR}$. Again, this provides important background information for the therapeutic manipulation of follicular apoptosis. Existing mouse mutants can be used to explore the intriguing possibility that neurotrophins and the low-affinity neurotrophin receptor are crucial for controlling not only neuronal[10,38] but also epithelial cell apoptosis.

The lack of convincing evidence from our study that $p55^{TNFR}$ and Fas, the two prototype cell surface receptors for apoptosis induction,[30,74,75] are responsible for determining where and when in the hair bulb keratinocytes are singled out to die further encourages one to systematically explore in the future the role of inhibitory controls of catagen-associated apoptosis. Possibly, apoptosis in the hair bulb is chiefly determined by a sudden decline during late anagen and catagen of local antiapoptotic stimuli that normally suppress apoptosis in the anagen hair bulb (cf Ref. 18). Also, the "apoptomap" generated here invites one to dissect to which extent different epithelial cell populations in the hair follicle use distinct apoptosis controls.[72] Certainly, the current study illustrates that the murine hair follicle offers a convenient, clinically relevant and most instructive necrobiological research tool for studying the social and intracellular controls of epithelial cell apoptosis *in situ* under physiological and pathological conditions.

Acknowledgments

We thank Prof. W. Sterry for his support and encouragement; R. Pliet, E. Hagen, M. Schilli, and R. Böhmer for excellent technical assistance; and Dr. S. Eichmüller for helpful advice.

References

1. Straile W, Chase H, Arsenault C: Growth and differentiation of hair follicles between periods of activity and quiescence. J Exp Zool 1961, 148:205–221
2. Parakkal PF: Ultrastructural changes of the basal lamina during the hair growth cycle. J Cell Biol 1969, 40:561–564
3. Weedon D, Strutton G: Apoptosis as the mechanism of the involution of hair follicles in catagen transformation. Acta Dermatol Venereol 1981, 61:335–339
4. Paus R, Rosenbach T, Haas N, Czarnetzki BM: Patterns of cell death: the significance of apoptosis for dermatology. Exp Dermatol 1993, 2:3–11
5. Polakowska RR, Haake AR: Apoptosis: the skin from a new perspective. Cell Death Differ 1994, 1:19–31
6. Gilbert S: Developmental Biology. Sinauer, Sunderland, MA
7. Polakowska RR, Piacentini M, Bartlett R, Goldsmith LA, Haake AR: Apoptosis in human skin development: morphogenesis, periderm, and stem cells. Dev Dyn 1994, 199:176–188
8. Gavrieli Y, Sherman Y, Ben Sasson SA: Identification of programmed cell death in situ via specific labeling of nuclear DNA fragmentation. J Cell Biol 1992, 119:493–501
9. Cotter SJ, Martin TG: Techniques in Apoptosis. London, Portland Press, 1996
10. Schwartz L, Milligan C: Cold thoughts of death: the role of ICE proteases in neuronal cell death. Trends Neurosci 1996, 19:555–562
11. Nagata S, Golstein P: The Fas death factor. Science 1995, 267:1449–1456
12. Golstein P: Controlling cell death. Science 1997, 275:1081–1082
13. White E: Life, death, and the pursuit of apoptosis. Genes Dev 1996, 10:1–15
14. Schwarz A, Bhardwaj R, Aragane Y, Mahnke K, Riemann H, Metze D, Luger TA, Schwarz T: Ultraviolet-B-induced apoptosis of keratinocytes: evidence for partial involvement of tumor necrosis factor-α in the formation of sunburn cells. J Invest Dermatol 1995, 104:922–927
15. Seiberg M, Marthinuss J, Stenn KS: Changes in expression of apoptosis-associated genes in skin mark early catagen. J Invest Dermatol 1995, 104:78–82
16. Moore GP, Panaretto BA, Carter NB: Epidermal hyperplasia and wool follicle regression in sheep infused with epidermal growth factor. J Invest Dermatol 1985, 84:172–175
17. Hollis DE, Chapman RE: Apoptosis in wool follicles during mouse epidermal growth factor (mEGF)-induced catagen regression. J Invest Dermatol 1987, 88:455–458
18. Paus R: Control of the hair cycle and hair diseases as cycling disorders. Curr Opin Dermatol 1996, 3:248–258
19. Stenn KS, Combates NJ, Eilertsen KJ, Gordon JS, Pardinas JR,

Parimoo S, Prouty SM: Hair follicle growth controls. Dermatol Clin 1996, 14:543–558
20. Raff MC, Barres BA, Burne JF, Coles HS, Ishizaki Y, Jacobson MD: Programmed cell death and the control of cell survival: lessons from the nervous system. Science 1993, 262:695–700
21. Kroemer G, Petit P, Zamzami N, Vayssiere JL, Mignotte B: The biochemistry of programmed cell death. FASEB J 1995, 9:1277–1287
22. Studzinski GP: Cell Growth and Apoptosis. Oxford, Oxford University Press, 1995
23. Chinnaiyan AM, Orth K, O'Rourke K, Duan H, Poirier GG, Dixit VM: Molecular ordering of the cell death pathway. Bcl-2 and Bcl-xL function upstream of the CED-3-like apoptotic proteases. J Biol Chem 1996, 271:4573–4576
24. Seiberg M, Marthinuss J: Clusterin expression within skin correlates with hair growth. Dev Dyn 1995, 202:294–301
25. Paus R, Hofmann U, Eichmüller S, Czarnetzki BM: Distribution and changing density of γ-delta T cells in murine skin during the induced hair cycle. Br J Dermatol 1994, 130:281–289
26. Paus R, Stenn KS, Link RE: Telogen skin contains an inhibitor of hair growth. Br J Dermatol 1990, 122:777–784
27. Paus R, Handjiski B, Czarnetzki BM, Eichmüller S: A murine model for inducing and manipulating hair follicle regression (catagen): effects of dexamethasone and cyclosporin A. J Invest Dermatol 1994, 103: 143–147
28. Slominski A, Paus R, Plonka P, Chakraborty A, Maurer M, Pruski D, Lukiewicz S: Melanogenesis during the anagen-catagen-telogen transformation of the murine hair cycle. J Invest Dermatol 1994, 102:862–869
29. Oltvai ZN, Milliman CL, Korsmeyer SJ: Bcl-2 heterodimerizes in vivo with a conserved homolog, Bax, that accelerates programmed cell death. Cell 1993, 74:609–619
30. Fraser A, Evan G: A license to kill. Cell 1996, 85:781–784
31. Enari M, Talanian RV, Wong WW, Nagata S: Sequential activation of ICE-like and CPP32-like proteases during Fas-mediated apoptosis. Nature 1996, 380:723–726
32. Kitson J, Raven T, Jiang YP, Goeddel DV, Giles KM, Pun KT, Grinham CJ, Brown R, Farrow SN: A death-domain-containing receptor that mediates apoptosis. Nature 1996, 384:372–375
33. Huang B, Eberstadt M, Olejniczak ET, Meadows RP, Fesik SW: NMR structure and mutagenesis of the Fas (APO-1/CD95) death domain. Nature 1996, 384:638–641
34. Smith CA, Farrah T, Goodwin RG: The TNF receptor superfamily of cellular and viral proteins: activation, costimulation, and death. Cell 1994, 76:959–962
35. Cleveland JL, Ihle JN: Contenders in FasL/TNF death signaling. Cell 1995, 81:479–482
36. Frade JM, Rodriguez-Tebar A, Barde YA: Induction of cell death by endogenous nerve growth factor through its p75 receptor. Nature 1996, 383:166–168
37. Casaccia-Bonnefil P, Carter BD, Dobrowsky RT, Chao MV: Death of oligodendrocytes mediated by the interaction of nerve growth factor with its receptor p75. Nature 1996, 383:716–719
38. Davies AM: Neurotrophins: The yin and yan of nerve growth factor. Curr Biol 1997, 7:38–40
39. Paus R, Handjiski B, Eichmüller S, Czarnetzki BM: Chemotherapy-induced alopecia in mice: induction by cyclophosphamide, inhibition by cyclosporine A, and modulation by dexamethasone. Am J Pathol 1994, 144:719–734
40. Paus R, Schilli MB, Handjiski B, Menrad A, Henz BM, Plonka P: Topical calcitriol enhances normal hair regrowth but does not prevent chemotherapy-induced alopecia in mice. Cancer Res 1996, 56: 4438–4443
41. Slominski A, Paus R, Plonka P, Handjiski B, Maurer M, Chakraborty A, Mihm MC: Pharmacological disruption of hair follicle pigmentation by cyclophosphamide as a model for studying the melanocyte response to and recovery from cytotoxic drug damage in situ. J Invest Dermatol 1996, 106:1203–1211
42. Goldberg MT, Tackaberry LE, Hardy MH, Noseworthy JH: Nuclear aberrations in hair follicle cells of patients receiving cyclophosphamide: a possible in vivo assay for human exposure to genotoxic agents. Arch Toxicol 1990, 64:116–121
43. Cece R, Cazzaniga S, Morelli D, Sfondrini L, Bignotto M, Menard S, Colnaghi MI, Balsari A: Apoptosis of hair follicle cells during doxorubicin-induced alopecia in rats. Lab Invest 1996, 75:601–609
44. Kaufmann SH: Proteolytic cleavage during chemotherapy induced apoptosis. Mol Med Today 1996, 2:298–303
45. Fearnhead HO, MacFarlane M, Dinsdale D, Cohen GM: DNA degradation and proteolysis in thymocyte apoptosis. Toxicol Lett 1995, 83:135–141
46. Zhivotovsky B, Gahm A, Ankarcrona M, Nicotera P, Orrenius S: Multiple proteases are involved in thymocyte apoptosis. Exp Cell Res 1995, 221:404–412
47. Gong J, Traganos F, Darzynkiewicz Z: A selective procedure for DNA extraction from apoptotic cells applicable for gel electrophoresis and flow cytometry. Anal Biochem 1994, 218:314–319
48. Eichmüller S, Stevenson PA, Paus R: A new method for double immunolabelling with primary antibodies from identical species. J Immunol Methods 1996, 190:255–265
49. Botchkarev VA, Eichmüller S, Peters EM, Johansson O, Maurer M, Paus R: A simple immunofluorescence technique for simultaneous visualization of mast cells and nerve fibers reveals selectivity and hair cycle-dependent changes in mast cell-nerve fiber contacts in murine skin. Arch Dermatol Res 1997, 289:292–302
50. Shimizu S, Eguchi Y, Kamiike W, Matsuda H, Tsujimoto Y: Bcl-2 expression prevents activation of the ICE protease cascade. Oncogene 1996, 12:2251–2257
51. Bhat RV, DiRocco R, Marcy VR, Flood DG, Zhu Y, Dobrzanski P, Siman R, Scott R, Contreras PC, Miller M: Increased expression of IL-1β converting enzyme in hippocampus after ischemia: selective localization in microglia. J Neurosci 1996, 16:4146–4154
52. Handjiski BK, Eichmüller S, Hofmann U, Czarnetzki BM, Paus R: Alkaline phosphatase activity and localization during the murine hair cycle. Br J Dermatol 1994, 131:303–310
53. Pierard-Franchimont C, Pierard GE: Massive lymphocyte-mediated apoptosis during the early stage of pseudopelade. Dermatologica 1986, 172:254–257
54. Potten CS: Cell death (apoptosis) in hair follicles and consequent changes in the width of hairs after irradiation of growing follicles. Int J Radiat Biol Relat Stud Phys Chem Med 1985, 48:349–360
55. Geng L, Potten CS: Changes after irradiation in the number of mitotic cells and apoptotic fragments in growing mouse hair follicles and in the width of their hairs. Radiat Res 1990, 123:75–81
56. Paus R, Menrad A, Czarnetzki BM: Nekrobiologie der Haut. Hautarzt 1995, 46:285–303
57. Lasic DD, Papahadjopoulos D: Liposomes revisited. Science 1995, 267:1275–1276
58. Li L, Hoffman RM: The feasibility of targeted selective gene therapy of the hair follicle. Nature Med 1995, 1:705–706
59. Hug P, Sleight RG: Liposomes for the transformation of eukaryotic cells. Biochim Biophys Acta 1991, 1097:1–17
60. Cotsarelis G, Sun TT, Lavker RM: Label-retaining cells reside in the bulge area of pilosebaceous unit: implications for follicular stem cells, hair cycle, and skin carcinogenesis. Cell 1990, 61:1329–1337
61. Stenn KS, Lawrence L, Veis D, Korsmeyer S, Seiberg M: Expression of the bcl-2 protooncogene in the cycling adult mouse hair follicle. J Invest Dermatol 1994, 103:107–111
62. Cosulich SC, Green S, Clarke PR: Bcl-2 regulates activation of apoptotic proteases in a cell-free system. Curr Biol 1996, 6:997–1005
63. Chase H: Growth of the hair. Physiol Rev 1954, 34:113–126
64. Hardy MH: The secret life of the hair follicle. Trends Genet 1992, 8:55–61
65. Kroemer G, Zamzami N, Susin N: Mitochondrial control of apoptosis. Immunol Today 1997, 18:44–51
66. Akbar AN, Salmon M: Cellular environments and apoptosis: tissue microenvironments control activated T cell death. Immunol Today 1997, 18:72–76
67. Hockenbery DM: bcl-2 in cancer, development and apoptosis. J Cell Sci Suppl 1994, 18:51–55
68. Sentman CL, Shutter JR, Hockenbery D, Kanagawa O, Korsmeyer SJ: bcl-2 inhibits multiple forms of apoptosis but not negative selection in thymocytes. Cell 1991, 67:879–888
69. Giannakis C, Forbes IJ, Zalewski PD: Ca2+/Mg(2+)-dependent nuclease: tissue distribution, relationship to inter-nucleosomal DNA fragmentation and inhibition by Zn2+. Biochem Biophys Res Commun 1991, 181:915–920
70. Morana S, Li J, Springer EW, Eastman A: The inhibition of etoposide-

induced apoptosis by zinc is associated with modulation of intracellular pH. Int J Oncol 1994, 5:153–158
71. Plonka P, Handjiski B, Plonka B, Paus R: Ambivalent effects of oral zinc on normal and dystrophic murine hair growth and pigmentation. J Invest Dermatol 1997, 108:652a
72. Mitra RS, Wrone-Smith T, Simonian P, Foreman K, Nunez G, Nickoloff BJ: Apoptosis in keratinocytes is not dependent on induction of differentiation. Lab Invest 1997, 76:99–107
73. Tamada Y, Takama H, Kitamura T, Yokochi K, Nitta Y, Ikeya T, Matsumoto Y: Identification of programmed cell death in normal human skin tissues by using specific labelling of fragmented DNA. Br J Dermatol 1994, 131:4521–4521
74. Nagata S: Apoptosis by death factor. Cell 1997, 88:355–365
75. Chinnaiyan AM, Tepper CG, Seldin MF, O'Rourke K, Kischkel FC, Hellbardt S, Krammer PH, Peter ME, Dixit VM: FADD/MORT1 is a common mediator of CD95 (Fas/APO-1) and tumor necrosis factor receptor-induced apoptosis. J Biol Chem 1996, 271:4961–4965
76. Veis DJ, Sorenson CM, Shutter JR, Korsmeyer SJ: Bcl-2-deficient mice demonstrate fulminant lymphoid apoptosis, polycystic kidneys, and hypopigmented hair. Cell 1993, 75:229–240
77. Krajewski S, Krajewska M, Shabaik A, Miyashita T, Wang HG, Reed JC: Immunohistochemical determination of in vivo distribution of Bax, a dominant inhibitor of Bcl-2. Am J Pathol 1994, 145:1323–1336
78. Ogasawara J, Suda T, Nagata S: Selective apoptosis of CD4+CD8+ thymocytes by the anti-Fas antibody. J Exp Med 1995, 181:485–491
79. Engelmann H, Novick D, Wallach D: Two tumor necrosis factor-binding proteins purified from human urine: evidence for immunological cross-reactivity with cell surface tumor necrosis factor receptors. J Biol Chem 1990, 265:1531–1536
80. Bothwell M: P75(Ntr): receptor after all. Science 1996, 272:506–507
81. Welker P, Foitzik K, Bulfone-Paus S, Henz BM, Paus R: Hair cycle dependent changes in the gene expression and protein content of transforming growth factor β 1 and β 3. Arch Dermatol Res 1997, 289:554–557